Progress In Electromagnetics Research, Vol. 126, 499–519, 2012

A COMPARISON BETWEEN PML, INFINITE ELEMENTS AND AN ITERATIVE BEM AS MESH TRUNCATION METHODS FOR *HP* SELF-ADAPTIVE PROCEDURES IN ELECTROMAGNETICS

I. Gomez-Revuelto [1], L. E. Garcia-Castillo [2, *], and L. F. Demkowicz [3]

[1]Dpto. Ingeniería Audiovisual y Com., Universidad Politénica de Madrid, E.U.I.T.T Ctra. Valencia Km. 7, Madrid 28031, Spain

[2]Dpto. Teoría de la Señal y Com., Universidad Carlos III de Madrid, Escuela Politécnica Superior, Avda. de la Universidad, 30, Leganés, Madrid 28911, Spain

[3]Institute for Computational Engineering and Sciences (ICES), University of Texas, Austin, USA

Abstract—Finite element *hp*-adaptivity is a technology that allows for very accurate numerical solutions. When applied to open region problems such as radar cross section prediction or antenna analysis, a mesh truncation method needs to be used. This paper compares the following mesh truncation methods in the context of *hp*-adaptive methods: Infinite Elements, Perfectly Matched Layers and an iterative boundary element based methodology. These methods have been selected because they are exact at the continuous level (a desirable feature required by the extreme accuracy delivered by the *hp*-adaptive strategy) and they are easy to integrate with the logic of *hp*-adaptivity. The comparison is mainly based on the number of degrees of freedom needed for each method to achieve a given level of accuracy. Computational times are also included. Two-dimensional examples are used, but the conclusions are directly extrapolated to the three dimensional case.

Received 2 February 2012, Accepted 23 March 2012, Scheduled 4 April 2012

* Corresponding author: Luis E. Garcia-Castillo (luise@tsc.uc3m.es).

1. INTRODUCTION

The use of "adapted" meshes [1], not only to the geometry of the problem domain, but to the solution of the problem itself, is a powerful feature of the Finite Element Method (FEM) [2–7]. Finite element *hp*-adaptivity is a technology that, by means of simultaneous *h*-refinements (modification of element size) and *p*-refinements (variation of the polynomial order or approximation *p*), it delivers very accurate numerical solutions. Actually, it provides exponential rates of convergence even in the presence of singularities, in contrast to *h* and *p* adaptive schemes, in which only algebraic rates of convergence are, in general, obtained. An illustration of the differences between the mentioned types of adaptive strategies is shown in Fig. 1.

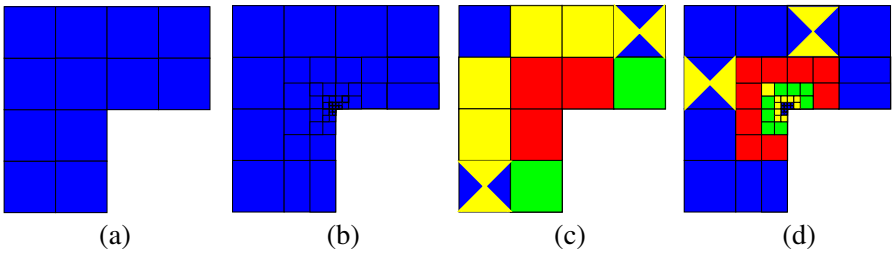

Figure 1. Different types of refinements. Different colors indicate the polynomial order *p* of approximation of the elements (blue being $p = 1$ and orange $p = 6$). (a) Given initial mesh. (b) *h*-refined mesh. (c) *p*-refined mesh. (d) *hp*-refined mesh.

The use of *h*-adaptivity is relatively common within the electrical engineering community (see [3] and references therein). However, *p* and *hp* adaptivity are rarely utilized, despite the intensive research performed during the last two decades in the development of hierarchical higher order curl-conforming basis (e.g., see [8–12]). During the last years, the authors have developed a fully automatic *hp*-adaptivity for electromagnetic problems (see [13, 14] and references therein) with applications to microwave engineering and scattering-radiation problems [15, 16].

In contrast to boundary element formulations [17, 18], finite element formulations have as unknown the electromagnetic field (and not its sources). Thus, when dealing with open region problems, as in the case of scattering and radiation of electromagnetic waves, the problem domain is infinite. Several approaches can be used in order to make the number of degrees of freedom finite after the discretization stage. Typically, the original infinite domain is decomposed into one

finite (interior) domain and one infinite (exterior) domain.

One approach is to use a non-standard FEM discretization of the infinite exterior domain with infinite elements [19].

Other approach is the integral equation representation of the field in the infinite domain by using boundary elements [20] on the interface between the exterior and interior domains. Thus, this interface becomes an artificial boundary that is used to truncate the problem domain (mesh) in order to keep the number of unknowns finite. Boundary elements provide an exact radiation boundary condition at the artificial boundary, allowing for the FEM domain to be truncated very close to the sources of the problem and, hence, reducing the number of unknowns of the problem. However, boundary element discretizations provide dense matrices.

Another truncation method consists of using *local* boundary conditions on the artificial boundary, whose discretization yields to sparse matrices. They are referred to as Absorbing Boundary Conditions (ABCs) [21–25]. However, ABCs are obtained using several approximations and are not exact, even at the continuous level (before discretization). In general, they are more accurate as the artificial boundary is placed at a longer distance from the sources. There exist several numerical techniques to obtain local ABCs, such as the so called Numerical ABC (NABC) [26], and Measured Equation of Invariance (MEI) method [27]. It is also remarkable the use of adaptive ABCs in which a given local boundary condition is iteratively updated; typically using the information about the radiation boundary condition implicit in the Green's function corresponding to the integral form representation of the exterior field. See e.g., [3, Chap. 6, 7], [28–31].

Another domain truncation method is the inclusion of one or several layers of lossy material that does not produce any reflection of the waves, independently of the incidence angle, i.e., Perfectly Matched Layers (PML). Although PML materials are unphysical, they can be used for the numerical analysis of open problems. PML was first proposed in [32], and later reformulated in several ways [33, 34]. PML provide solutions which are arbitrarily exact at the continuous level. That is, the reflection can be made arbitrarily small (for any given PML thickness) by properly selecting the parameters of the PML profile. However, at the discrete level, this property could be seriously compromised. Indeed, PML may damage the accuracy and increase the conditioning of FEM solutions (e.g., see [35] and references therein). However, for the case of *hp*-adaptivity, the PML seems a good candidate to truncate the computational domain, as shown in [36, 37].

The main contribution of this paper is to compare available mesh truncation methods in electromagnetics that may be suitable

for *hp*-adaptivity. Due to the very high accuracy provided by the *hp*-adaptivity, truncation methods are required to be exact, or at least, they should be arbitrarily exact at the continuous level. It is also desirable for the mesh truncation techniques to provide an easy integration with the logic of the *hp*-adaptivity. Thus, the methods selected for the comparison are: Infinite Elements, PML, and the iterative boundary-based *hp* method described in [16]. Further details about each one of the mentioned methods will be given later. The main criteria for the comparison is the number of degrees of freedom (d.o.f.) needed by each method to achieve a given level of accuracy. Computational times will be also compared.

2. *HP*-ADAPTIVITY AND MESH TRUNCATION METHODS

The *hp*-FEM utilizes quadrangles/triangles of variable order of approximation supporting anisotropic refinements and *hanging nodes*. The adaptive strategy is fully automatic and is based on minimizing the interpolation error by using the projection of the error from a *fine grid*. This fine grid is obtained from a uniform refinement in h and p of the given coarse grid. The resulting *hp*-adaptive strategy delivers exponential convergence rates in terms of the energy error versus the number of d.o.f., even in the presence of singularities. For details see [13] and references therein.

In this paper, the adaptivity is applied to the scalar 2D Helmholtz problem consisting of the scattering of infinitely long z-oriented cylinders with TM and TE incidence polarized waves, i.e.,

$$\frac{\partial}{\partial x}\left(\frac{1}{f_r}\frac{\partial u}{\partial x}\right)+\frac{\partial}{\partial y}\left(\frac{1}{f_r}\frac{\partial u}{\partial y}\right)+k_0^2 g_r u = q \tag{1}$$

where $k_0 = \omega\sqrt{\mu_0\varepsilon_0}$ is the vacuum wavenumber, μ_0, ε_0 are the permittivity and permeability of vacuum, respectively. For TE polarization, $f_r = \varepsilon_r$, $g_r = \mu_r$ and u refers to the z-component of the magnetic field (for TM polarization, see [38]). Symbol q represents the interior sources. H^1-conforming finite elements using hierarchical basis functions based on integrated Legendre polynomials are used to discretize (1).

2.1. Infinite Element

The analysis with infinite elements is made by using a scattered field formulation enclosing the scatterer with a circular boundary of radius a. The infinite element extends from the enclosing boundary

up to infinity. In practice, it is displayed as an elongated element in the radial direction ρ. This setup can be identified in the *hp* meshes shown in Section 3. The basis functions of the infinite element are constructed by taking tensor products of one-dimensional radial shape functions $\psi(a/\rho)$ with the traditional (used within the interior domain) hierarchical basis functions corresponding to the edge lying on the truncating circle $e(\phi)$. Thus, the variation in the far-field region is factorized. The infinite element basis functions are expressed (assuming the enclosing boundary centered in the origin) as:

$$u(\rho,\phi) = \frac{e^{-jk(\rho-a)}}{\rho^{\frac{1}{2}}} \sum_j \sum_l g_{jl} e_l(\phi) \psi_j(a/\rho) \tag{2}$$

where coefficients g_{jl} denote the degrees of freedom. See [13] for details.

It is worth noting that the infinite element is not considered in the optimization procedure that yields to the next optimal mesh. Thus, no *h*-refinements are made in the radial direction. *h*-refinements are forced by the topology of the edges lying on the truncating circle. The order p in the radial direction is simply set to the p of the edge on the truncating circle plus one. In addition, there is a maximum p in practice ($p = 9$ in our code), that limits the accuracy of the approximation in the radial direction. Nonetheless, infinite elements are exact at the continuous level. However, the practical limitations of the implementation described above precludes an arbitrarily exact field modeling within the exterior domain. Another disadvantage is the need of a simple analytic type of truncating interface, such as a circle in 2D or sphere in 3D.

2.2. Perfectly Matched Layers (PML)

The analysis with PML is made by enclosing the scatterer with a PML of a given thickness at a given distance from the scatterer. The geometry is typically circular or rectangular. PML can be formulated in several ways. The most useful and elegant way is the one based on the concept of analytical continuation of a real function into the complex plane (referred to as *complex coordinate stretching* [39]). For instance, with rectangular box type PML, the stretching is made on the Cartesian coordinates as follows (analogous stretching with y):

$$x \quad \rightarrow \quad z_x(x) = x + a_x(x) - jb_x(x) \tag{3}$$

where $z_x(x)$ is the complex coordinate. Factor b_i takes care of the attenuation of propagating waves and factors a_i of the evanescent waves. In the domain of interest, $a_i = b_i = 0$ which yields $z_x(x) = x$ and thus, the original unstretched equations are recovered.

Mapping (3) is introduced into (1) and the stretching yields to complex material constants (see [36] for details). Different mappings can be selected yielding to different PML "profiles". For example, b_x could be set for a wave travelling in the positive x direction as:

$$b_x(x) = \frac{x}{C_1}\left(\frac{x - x_{\text{PML}}}{C_2}\right)^n, \quad x > x_{\text{PML}} \tag{4}$$

where x_{PML} indicates the beginning (in x) of the PML. It is easily deduced that the level of reflection of the PML can be arbitrarily small by properly selecting parameters C_1, C_2 and integer n. In addition, it is very simple to implement a PML within the *hp*-adaptive code; PML is simply another medium of the problem. Another advantage of PML is that it is suitable for mesh truncation in different types of problems without modifications, e.g., for multilayer structures. The drawback comes from the high number of extra degrees of freedom that have to be spent within the PML, as it will be clear later.

In contrast to the infinite element, finite elements within the PML region are taken into account in the self-adaptive algorithm. Thus, they are automatically refined in h and p at each step of the adaptivity. However, their contributions to the error are not taken into account in the comparison. Although *hp*-adaptivity has demonstrated to accurately resolve (in contrast to classical FE discretizations) the electromagnetic field, independently of the PML profile [36, 37], there is an optimum profile (in terms of the number of unknowns needed to achieve a given level of accuracy of the field solution), which is problem dependent.

2.3. Iterative Boundary Element Methodology (FE-IIEE)

The analysis with this mesh truncation technique is based on a two domain decomposition with overlapping approach. An iterative multiplicative Schwarz type algorithm is performed. A finite (interior) domain is obtained by enclosing the scatterer with an arbitrary (typically conformal) boundary (denoted by S). A FEM is used to model the field within this domain. A local type of boundary condition is used on S, e.g., a Cauchy type, $\partial u/\partial n + jk_0\, u = \Psi$ being its residual function Ψ assumed to be known.

An infinite (exterior) domain is obtained using an auxiliary boundary S' that is interior to S. Thus, the overlapping region is limited by S and S'. The field on S for next iteration is calculated using the Equivalence Principle on S':

$$u_{\text{sc}}{}^{(i+1)}\Big|_S = \oint_{S'} \left[M^t_{\text{eq}} \frac{\partial G}{\partial n'} - jk_0\eta_0 J^z_{\text{eq}}\, G \right] dl' \tag{5}$$

where M^t_{eq} and J^z_{eq} are the equivalent magnetic and electric currents, respectively, on S'. Superindexes t and z refer to the tangential and longitudinal components, respectively. Symbol G denotes the Green's function of the exterior domain (e.g., free space). The normal derivative $\partial u/\partial n$ on S is calculated in an analogous way and, thus, the residual Ψ of the boundary condition on S is updated. For details see [38]. This approach can be interpreted as an iterative implementation of a boundary element method in which no integral equation must be solved, but only "evaluated" (expression (5) and its analog for $\partial u/\partial n$). This technique will be referred to as FE-IIEE (Finite Element-Iterative Integral Equation Evaluation) in the rest of the paper.

FE-IIEE allows for the radiation boundary condition provided by the integral representation of the field to be imposed with an arbitrary accuracy (asymptotically exact with the number of iterations at the continuous level) without using boundary elements in the *hp*-adaptivity. A drawback of this method, in comparison with PML, is that it requires the use of the specific Green's function of the exterior domain [40]. Thus, for instance, when applied to stratified media, the multilayer Green's function [41] has to be implemented.

The use of FE-IIEE does not increase the order of the computational complexity of the *hp*-adaptivity with the number of degrees of freedom (provided a fast method is used to evaluate (5)) because the FE overhead of using IIEE reduces simply to forward and backward substitutions. In addition the number of extra forward and backward substitutions is small. This is due to the reutilization of the residual Ψ of previous instances. First, at each step j of the adaptivity the last residual Ψ of the previous step of the adaptivity is used to start the FE-IIEE iterations. Second, the discrete Ψ obtained in the last iteration of FE-IIEE of the coarse mesh is used to start the FE-IIEE iterations for the fine mesh. In practice, two extra iterations of the iterative FEM for the fine mesh have demonstrated to be enough to guide the adaptivity. For details see [16, 42]. However, as it will be clear later, the overhead due to the evaluation of the convolutional expressions as the one of (5) affects to the computational time.

3. NUMERICAL RESULTS

Results for TE and TM cases provide similar conclusions. Thus, only results for the TE case are shown. Very coarse meshes with uniform order $p = 2$ have been used as initial meshes. The error is measured in the H^1 semi-norm only within the finite (interior) domain, which is the region of interest. That is, the error contributions of infinite elements

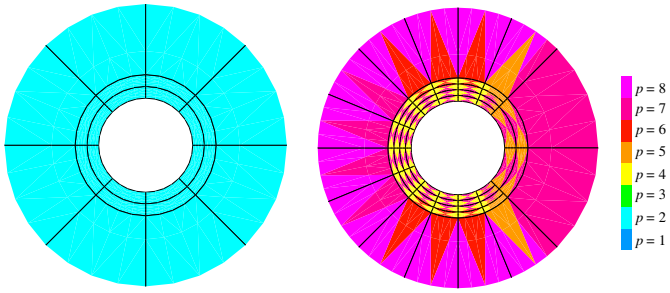

Figure 2. Scattering on PEC circular cylinder (*hp*-meshes with infinite elements). (a) Initial mesh. (b) 11th *hp*-mesh. $\varepsilon \simeq 0.01\%$.

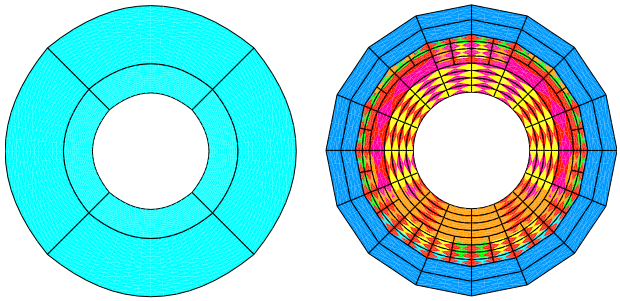

Figure 3. Scattering on PEC circular cylinder (*hp*-meshes with PML). (a) Initial mesh. (b) 18th *hp*-mesh. $\varepsilon \simeq 0.01\%$.

as well as those within the PML are not taken into account. Note again that finite elements in the PML region are taken into account in the self-adaptive algorithm to yield the next *hp* mesh.

The first scatterer is a circular cross-section metallic cylinder of radius equal to one wavelength (λ) illuminated from the right as displayed in the figures mentioned below. The cylinder surface is a perfect electric conductor (PEC).

The analysis with infinite elements is performed by placing a layer of infinite elements on a circular enclosing boundary at a distance equal to 0.5λ from the metallic cylinder boundary. The initial mesh and some of the *hp*-meshes provided by the adaptivity are shown in Fig. 2, in which colors indicates, according to the scale on the right (used also for the rest of the mesh plots), the order p of the elements. Due to the smoothness of the solution, the *hp*-adaptivity automatically selects p-refinements. Since the maximum p is limited in our implementation

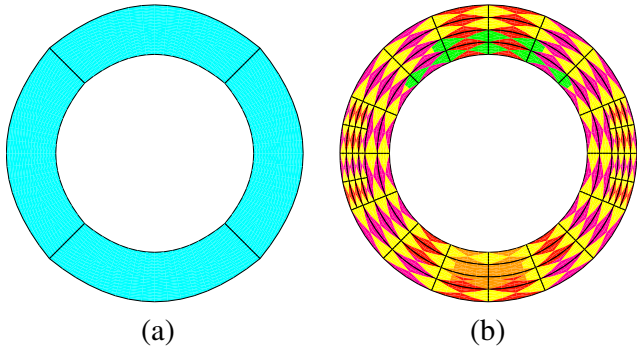

Figure 4. Scattering on PEC circular cylinder (*hp*-meshes for FE-IIEE). (a) Initial mesh. (b) 18th *hp*-mesh. $\varepsilon \simeq 0.01\%$.

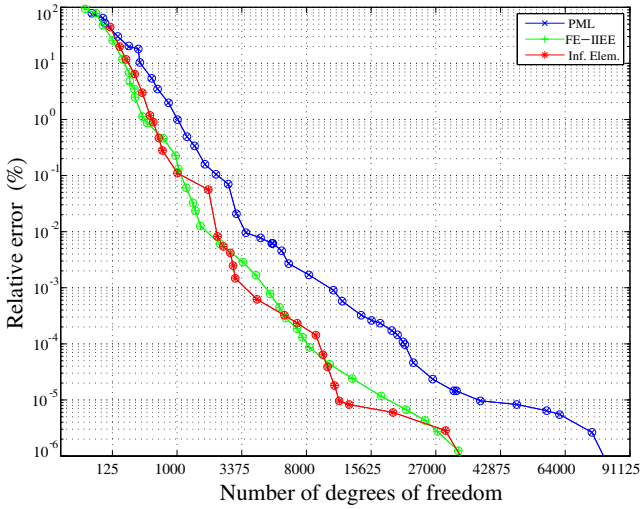

Figure 5. Scattering on PEC circular cylinder (convergence history).

by $p \leq 9$, once the maximum p is reached, h-refinements are selected. Fig. 5 describes the error history obtained with the sequence of *hp*-meshes provided by the self-adaptive algorithm. The marks with the circles correspond to the exact error measured with respect to the exact solution. Marks without circles correspond to the estimated error. The error estimation provided by the *hp*-adaptivity is highly accurate. Note that the abscissa scale corresponds to $N_{\text{dof}}^{1/3}$ (being N_{dof} the number of degrees of freedom) while abscissa axis tics should be read as N_{dof} in the plots. This is due to the fact that, according to [43],

error $= C\exp(-N_{\text{dof}}^{\alpha})$ (with $\alpha = 1/3$ for 2D) in the asymptotic regime. Thus, the exponential convergence behavior is identified by a straight line in the plot. In this case, the convergence presents different changes in the slopes due to the limitation on the maximum p mentioned above.

The analysis with PML is performed by placing a conformal PML region starting at 0.5λ away from the scatterer. A linear profile for $b(\rho)$ (i.e., $n = 1$ is set in an analogous mapping as (4) but with the radial coordinate ρ) was selected to be optimal for this case. The profile was designed for a (2 way) attenuation of approximately 70 dBs being $a(\rho)$ of expression (3) set to zero. The initial mesh and some of the *hp*-meshes provided by the adaptivity are displayed in Fig. 3, exhibiting a boundary layer type of behavior due to the presence of a PML. Note that, due to the use of isoparametric elements and the low error at the end of the PML (where the field is basically null), the geometry of the PML external boundary is modeled by straight lines. Fig. 5 describes the convergence history. The achieved error levels are very low. However, a PML requires a larger number of degrees of freedom. In average, between 40% and 80% of the total number of degrees of freedom are placed in the PML region when the PML is located in the proximity of the scatter (see Fig. 6 for a distance PML-scatter equal to 0.1λ).

The analysis with FE-IIEE is performed by placing a conformal truncation boundary at 0.5λ away from the scatterer. The initial mesh and one of the *hp*-meshes is shown in Fig. 4. There are no finite elements on the exterior domain; thus, the number of degrees of freedom are only those needed to model the field within the finite (interior) domain. This has a positive impact in the number of degrees of freedom needed for a given error level, as observed in the convergence history shown in Fig. 5.

As example of elongated structure, the scattering of an elliptical PEC cylinder illuminated by a plane wave coming from $\phi = 90^{\circ}$, was selected. The truncation boundary is a circle with infinite elements, a rectangle for PML, and conformal to the scatterer (an ellipse) for FE-IIEE. An illustration of the setup is shown in Fig. 7. The dimensions are indicated in the caption. Examples of the *hp*-meshes delivered by the automatic adaptivity are shown in Fig. 8, Fig. 9, and Fig. 10, for infinite elements, PML and FE-IIEE, respectively. By simple inspection of the meshes, a lower performance of infinite elements with respect to PML and FE-IIEE in terms of error versus number of degrees of freedom is expected. This is confirmed in Fig. 11, which shows the convergence history for the three methods.

The last example is the scattering of a rectangular PEC cylinder (dimensions equal to $8\lambda \times 1\lambda$) illuminated by a plane wave coming

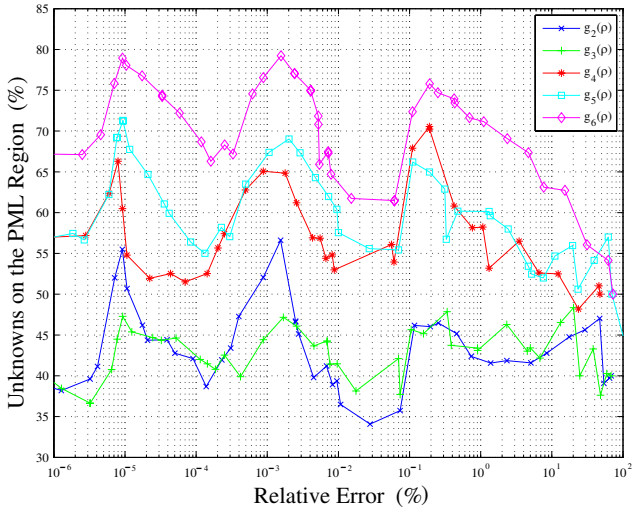

Figure 6. Percentage of degrees of freedom in the PML region depending on the PML profile used (case of PEC circular cylinder): $g_1(\rho) = 0.2\,(\rho - b)$; $g_2(\rho) = 2\,(\rho - b)$; $g_i(\rho) = \dfrac{\rho}{2^{(n(i)-1)}c}\left(\dfrac{\rho - b}{0.5}\right)^{n(i)}$; $n(3) = 1$, $n(4) = 3$, $n(5) = 5$, $n(6) = 15$ being b the radius where the PML starts.

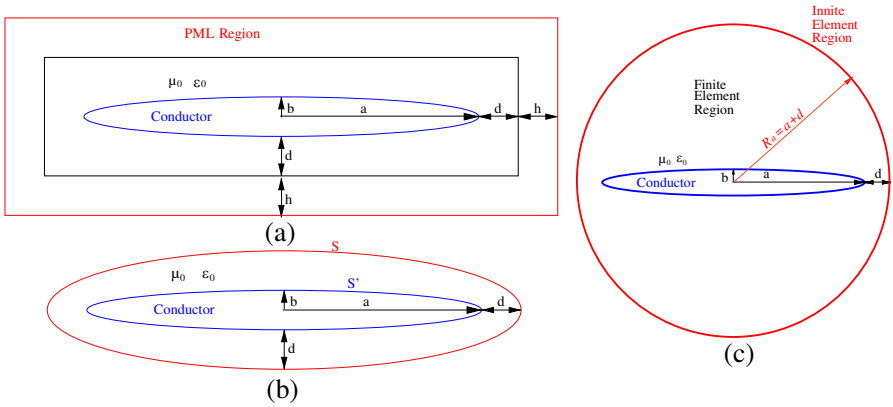

Figure 7. Set-up for PEC elliptical cylinder $a = 5\lambda$, $b = 0.5\lambda$, $R_a = 6\lambda$, $d = \lambda$, $h = \lambda$. Incidence from above. (a) PML. (b) IIEE. (c) Inf. Elem.

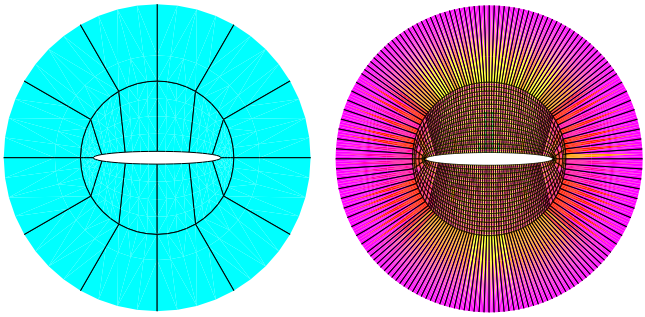

Figure 8. Scattering on PEC elliptical cylinder (*hp*-meshes with infinite elements). (a) Initial mesh. (b) 39th *hp*-mesh. $\varepsilon \simeq 1\%$.

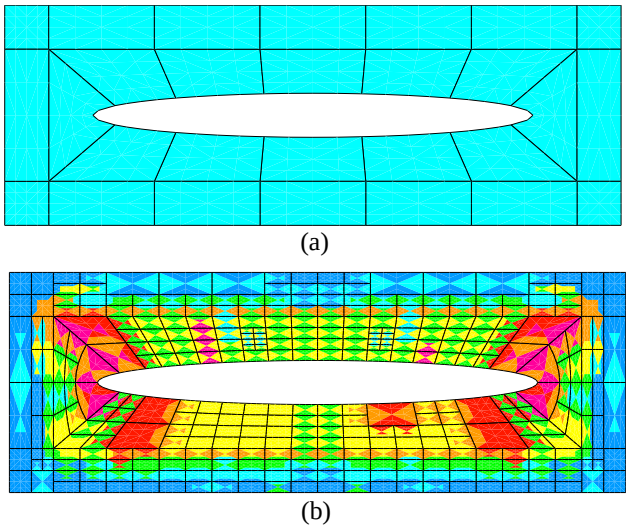

Figure 9. Scattering on PEC elliptical cylinder (*hp*-meshes with PML). (a) Initial mesh. (b) 18th *hp*-mesh. $\varepsilon \simeq 1\%$.

from $\phi = 90°$. It is an example of an elongated structure but, in contrast with previous structures, its solution is no longer smooth due to the field singularities ocurring at the corners of the scatterer. The truncation boundary is a circle (of radius 6λ) with infinite elements, and conformal to the scatterer (at 1.5λ from the scatterer) for FE-IIEE and PML. The convergence history for the three methods is shown in Fig. 12. It is observed that, despite the field singularities, exponential convergence is achieved. A stagnation with infinite elements is observed

close to an error level of 0.1%. Similar conclusions to the ones of previous structures hold with respect the performance of PML and FE-IIEE. The performance of infinite elements deteriorates due to the non smoothness of the solution and the need of a circle boundary to enclose the elongated scatterer.

Results corresponding to a distance between the scatterer and the

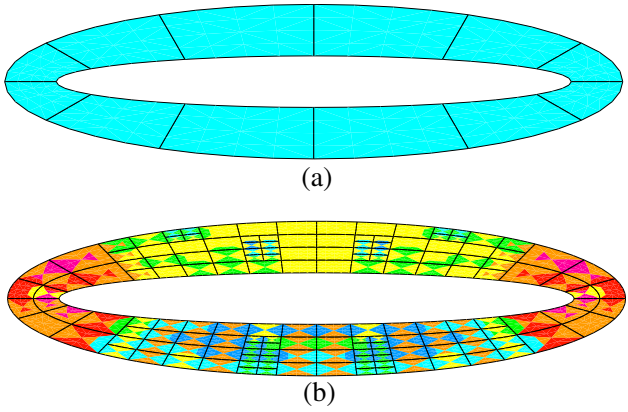

Figure 10. Scattering on PEC elliptical cylinder (*hp*-meshes with FE-IIEE). (a) Initial mesh. (b) 14th *hp*-mesh. $\varepsilon \simeq 1\%$.

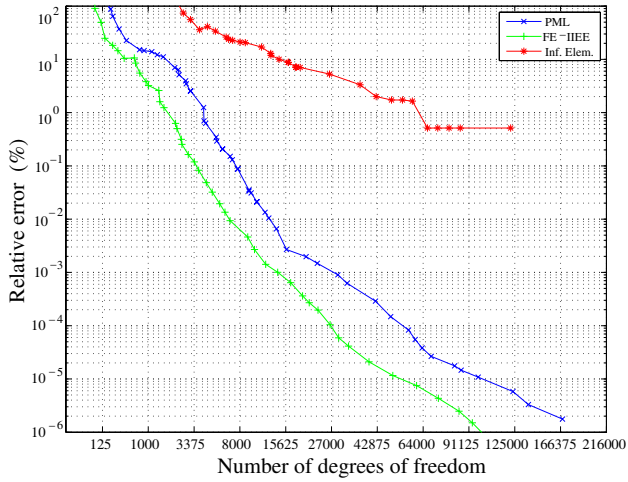

Figure 11. Scattering on PEC elliptical cylinder (convergence history).

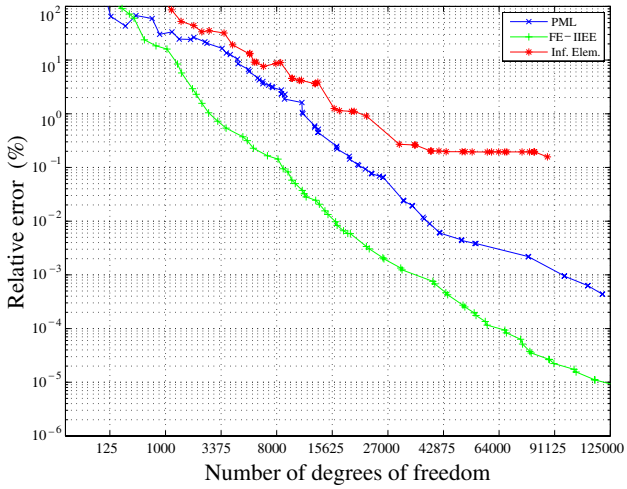

Figure 12. Scattering on PEC elongated rectangular cylinder (convergence history).

truncation boundary within 0.5λ–1.5λ have been shown. The main reason for not using shorter distances has been to use the same distance (for a given structure) for the three methods under comparison. As explained below, the limitations have come by the accuracy when using infinite elements. Another reason is simply graphical in the sense that meshes with very thin layers of finite elements would have been displayed in the paper. Additional results with much shorter distances 0.05λ–0.2λ have also been computed. In general, it has been observed that when infinite elements are placed very close to arbitrary scatterers, the *hp*-adaptivity demands *h*-refinements of the infinite elements in the radial direction. This feature is not available in practice due to its complexity. Equivalently, the infinite element layer might be placed further away from the scatterer. However, the implementation of that feature to be performed automatically (without user interaction) would unnecessarily complicate the code. In addition, it would add a high number of extra degrees of freedom to the analysis. On the other hand, the percentage of degrees of freedom in the PML region with respect to the total is getting higher as the PML is getting closer to the scatterer (i.e., the non-PML region is getting smaller). Thus, PML performs worse than FE-IIEE under these conditions.

The sparsity patterns of the FEM matrices obtained with the three methods do not show significant differences. Additionally, the three methods delivered a similar number of *hp*-iterations in order to obtain

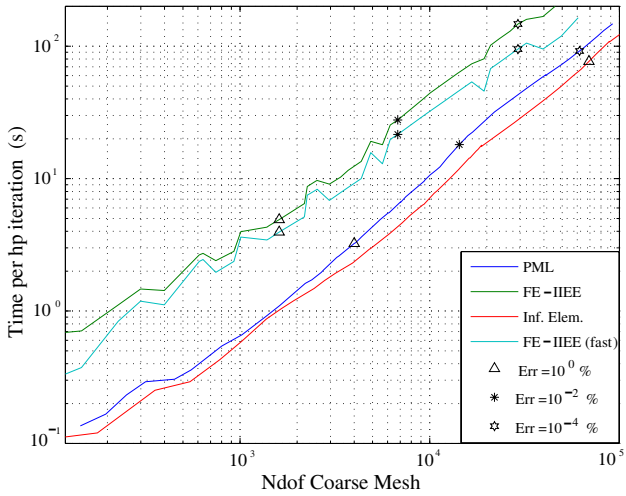

Figure 13. Computational time (in seconds) per *hp*-iteration for the elliptical cylinder.

Table 1. Accumulated computational time (in seconds) for the elliptical cylinder.

	Inf. Elem.	PML	FE-IIEE	FE-IIEE (fast)
Err = 10%	125	5	9	7
Err = 1%	554	20	34	28
Err = 0.1%	-	69	88	72
Err = 0.01%	-	155	204	160
Err = 0.001%	-	338	402	306
Err = 0.0001%	-	798	1049	730

meshes with a given number of degrees of freedom. This was expected, since the *hp*-adaptive strategy was the same for the three methods. Thus, the comparison has been based on the number of degrees of freedom of the last *hp* mesh needed to obtain a given level of accuracy.

The dependence of the computational time per *hp*-iteration with the number of degrees of freedom (of the coarse mesh) for the elliptical cylinder is shown in Fig. 13. The accumulated time considering all iterations needed for a given level of accuracy is shown in Table 1. Fig. 13 (with loglog axis) shows that the slope of the three methods is the same because they all use the same finite element solver. However, the overhead of FE-IIEE corresponding to the brute-force

accurate evaluation of the convolutional type operation of (5) (and its analogous for the normal derivative) is reflected as a shift of the FE-IIEE line towards larger computational times. Although the development of an efficient implementation of an acceleration technique (as FMM (*Fast Multipole Method* [44–46]) or ACA (*Adaptive Cross Approximation* [47]) using the hierarchy of the meshes (tree type data structures) is out of the scope of this paper, an estimation of the performance of FE-IIEE with an acceleration technique has been included. It corresponds to the line labeled as "FE-IIEE (fast)". The estimation of the computation time has been performed by considering a dependence of the type $O(N_\Gamma^{1.5})$ corresponding to a single level implementation (instead of $O(N_\Gamma^2)$ of the brute-force approach), being N_Γ the number of degrees of freedom of the exterior boundary. Based on this estimate, the computational time of FE-IIEE for large number of degrees of freedom is comparable to the ones of PML and infinite elements. The introduction of the information about the convergence history of each method in Fig. 13 is performed through marks: $\triangle$, $*$, $\star$. Each mark corresponds to the number of degrees of freedom (and hence computational time) for a given error level. The PML and FE-IIEE require similar computational times (with a slight advantage of PML over FE-IIEE), while infinite elements are discarded due to the large computational time (a factor of 100 when compared with PML and FE-IIEE). Although PML and FE-IIEE yield similar computational times, FE-IIEE does it with a significant lower number of degrees of freedom and thus, it requires less memory than PML. This issue may be relevant with large 3D problems.

4. CONCLUSIONS

From the results of Section 3, the following conclusions are obtained. Infinite elements are only competitive with PML and FE-IIEE for a small set of specific cases, since infinite elements exhibit a lack of robustness. Both, PML and FE-IIEE, are suitable for accurate *hp* modeling of scattering problems requiring similar computational times to deliver results with a given level of accuracy. FE-IIEE requires a lower number of degrees of freedom than PML for a given level of accuracy, i.e., it requires less memory than PML. Also, FE-IIEE performs better than PML when the truncation boundary is close to the scatterer. In addition, the truncation boundary can be made conformal to the scatterer with FE-IIEE. However, FE-IIEE requires the Green's function of the exterior domain and the implementation of the convolutional type of operation (preferably by using some sort of fast method) to update the right hand side of the problem. In this

sense, PML is simpler to be implemented within the *hp*-adaptive code and it does not require specific implementations for different exterior domains (e.g., free space, stratified media, etc.). Thus, although FE-IIEE may perform better for specific problems, specially in 3D, the simplicity of PML and its good performance when discretized with *hp*-finite elements make PML the preferred option as mesh truncation method for general purpose *hp*-adaptive codes.

ACKNOWLEDGMENT

The authors want to thank the suggestions made by the reviewers that have significantly improved the paper.

This work has been supported by the Ministerio de Educacion y Ciencia, Spain, under Projects TEC2007-65214/TCM and TEC2010-18175/TCM.

REFERENCES

1. Rheinboldt, W. C. and I. Babuska, "Error estimates for adaptive finite element computations," *SIAM Journal of Numerical Analysis*, Vol. 15, 736–754, Aug. 1978.
2. Jin, J. M., *The Finite Element Method in Electromagnetics*, 2nd edition, John Wiley & Sons, Inc., 2002.
3. Salazar-Palma, M., T. K. Sarkar, L. E. García-Castillo, T. Roy, and A. R. Djordjevic, *Iterative and Self-Adaptive Finite-Elements in Electromagnetic Modeling*, Artech House Publishers, Inc., Norwood, MA, 1998.
4. Ping, X. W. and T. J. Cui, "Factorized sparse approximate inverse preconditioned conjugate gradient algorithm for finite element analysis of scattering problems," *Progress In Electromagnetics Research*, Vol. 98, 15–31, 2009.
5. Tian, J., Z. Q. Lv, X. W. Shi, L. Xu, and F. Wei, "An efficient approach for multifrontal algorithm to solve non-positive-definite finite element equations in electromagnetic problems," *Progress In Electromagnetics Research*, Vol. 95, 121–133, 2009.
6. Klopf, E. M., S. B. Manić, M. M. Ilíc, and B. M. Notaroš, "Efficient time-domain analysis of waveguide discontinuities using higher order FEM in frequency domain," *Progress In Electromagnetics Research*, Vol. 120, 215–234, 2011.
7. Trujillo-Romero, C. J., L. Leija, and A. Vera, "FEM modeling for performance evaluation of an electromagnetic oncology deep hyperthermia applicator when using monopole, inverted T, and

plate antennas," *Progress In Electromagnetics Research*, Vol. 120, 99–125, 2011.

8. Andersen, L. S. and J. L. Volakis, "Hierarchical tangential vector finite elements for tetrahedra," *IEEE Microwave and Guided Wave Letters*, Vol. 8, 127–129, Mar. 1998.
9. Webb, J. P., "Hierarchical vector basis functions of arbitrary order for triangular and tetrahedral finite elements," *IEEE Transactions on Antennas and Propagation*, Vol. 47, 1244–1253, Aug. 1999.
10. Sun, D. K., J. F. Lee, and Z. Csendes, "Construction of nearly orthogonal Nedelec bases for rapid convergence with multilevel preconditioned solvers," *SIAM Journal of Scientific Computing*, Vol. 23, No. 4, 1053–1076, 2003.
11. Zhu, Y. and A. C. Cangellaris, "Finite element basis functions spaces for tetrahedra elements," *Applied Computational Electromagnetics Society (ACES) Meeting*, Monterey, CA, USA, Mar. 2001.
12. Ilíc, M. M., A. Ž. Ilíc, and B. M. Notaroš, "Efficient large-domain 2-D FEM solution of arbitrary waveguides using p-refinement on generalized quadrilaterals," *IEEE Transactions on Microwave Theory and Techniques*, Vol. 53, 1377–1383, Apr. 2005.
13. Demkowicz, L., *Computing with hp Finite Elements. I. One- and Two-Dimensional Elliptic and Maxwell Problems*, Chapman & Hall/CRC Press, Taylor and Francis, 2007.
14. Demkowicz, L., J. Kurtz, D. Pardo, M. Paszynski, W. Rachowicz, and A. Zdunek, *Computing with hp Finite Elements. II Frontiers: Three Dimensional Elliptic and Maxwell Problems with Applications*, Chapman & Hall/CRC Press, Taylor and Francis, 2008.
15. García-Castillo, L. E., D. Pardo, and L. F. Demkowicz, "Energy-norm based and goal-oriented automatic *hp* adaptivity for electromagnetics. Application to the analysis of H-plane and E-plane rectangular waveguide discontinuities," *IEEE Transactions on Microwave Theory and Techniques*, Vol. 56, 3039–3049, Dec. 2008, doi: 10.1109/TMTT.2008.2007096.
16. Gómez-Revuelto, I., L. E. García-Castillo, D. Pardo, and L. F. Demkowicz, "A two-dimensional self-adaptive *hp* finite element method for the analysis of open region problems in electromagnetics," *IEEE Transactions on Magnetics*, Vol. 43, 1337–1340, Apr. 2007, doi: 10.1109/TMAG.2007.892413.
17. Shi, Y., X. Luan, J. Qin, C. Lv, and C. H. Liang, "Multilevel Green's function interpolation method solution of volume/surface integral equation for mixed conducting/bi-isotropic objects,"

Progress In Electromagnetics Research, Vol. 107, 239–252, 2010.

18. Lancellotti, V., B. P. de Hon, and A. G. Tijhuis, "Scattering from large 3-D piecewise homogeneous bodies through linear embedding via Green's operators and Arnoldi basis functions," *Progress In Electromagnetics Research*, Vol. 103, 305–322, 2010.
19. Bettess, P., "Infinite elements," *International Journal for Numerical Methods in Engineering*, Vol. 11, 54–64, 1977.
20. Silvester, P. P. and M. S. Hsieh, "Finite-element solution of 2-dimensional exterior-field problems," *IEE Proceedings-H (Microw. Antennas Propag.)*, Vol. 118, 1743–1747, Dec. 1971.
21. Mur, G., "Absorbing boundary conditions for the finite-difference approximation of the time-domain electromagnetic-field equations," *IEEE Transactions on Electromagnetic Compatibility*, Vol. 23, 377–382, Nov. 1981.
22. Engquist, B. and A. Majda, "Absorbing boundary conditions for the numerical simulation of waves," *Mathematics of Computation*, Vol. 31, 629–651, Jul. 1977.
23. Bayliss, A. and E. Turkel, "Radiation boundary conditions for wave-like equations," *Communications on Pure and Applied Mathematics*, Vol. 33, 707–725, 1980.
24. D'Angelo, J. and I. D. Mayergoyz, "Finite element methods for the solution of RF radiation and scattering problems," *Electromagnetics*, Vol. 10, 177–199, 1990.
25. Mittra, R. and O. Ramahi, "Absorbing boundary conditions for the direct solution of partial differential equations arising in electromagnetic scattering problems," *Progress In Electromagnetics Research*, Vol. 2, 133–173, 1990.
26. Gordon, R., R. Mittra, A. Glisson, and E. Michielssen, "Finite element analysis of electromagnetic scattering by complex bodies using an efficient numerical boundary condition for mesh truncation," *Electronic Letters*, Vol. 29, 1102–1103, 1993.
27. Mei, K. K., R. Pous, Z. Chen, and Y. W. Liu, "The measured equation of invariance: A new concept in field computations," *IEEE Antennas and Propagation Society International Symposium Digest*, Vol. 4, 2047–2048, Institute of Electrical and Electronics Engineer (IEEE), Chicago, Illinois, USA, Jul. 1992.
28. Alfonzetti, S., G. Borzi, and N. Salerno, "Iteratively-improved Robin boundary conditions for the finite element solution of scattering problems in unbounded domains," *International Journal for Numerical Methods in Engineering*, Vol. 42, 601–629, 1998.

29. Liu, J. and J. M. Jin, "A novel hybridization of higher order finite element and boundary integral methods for electromagnetic scattering," *IEEE Transactions on Antennas and Propagation*, Vol. 49, 1794–1806, Dec. 2001.
30. Gómez-Revuelto, I., L. E. García-Castillo, M. Salazar-Palma, and T. K. Sarkar, "Fully coupled hybrid method FEM/high-frequency technique for the analysis of radiation and scattering problems," *Microwave and Optical Technology Letters*, Vol. 47, 104–107, Oct. 2005.
31. Fernández-Recio, R., L. E. García-Castillo, I. Gómez-Revuelto, and M. Salazar-Palma, "Fully coupled hybrid FEM-UTD method using NURBS for the analysis of radiation problems," *IEEE Transactions on Antennas and Propagation*, Vol. 56, 774–783, Mar. 2008.
32. Berenger, J. P., "A perfectly matched layer for the absorption of electromagnetic waves," *Journal of Computational Physics*, Vol. 114, 185–200, Oct. 1994.
33. Chew, W. C. and W. H. Weedon, "A 3-D perfectly matched medium from modified Maxwell's equations with stretched coordinates," *Microwave and Optical Technology Letters*, 599–604, 1994.
34. Sacks, Z. S., D. M. Kingsland, R. Lee, and J. F. Lee, "A perfectly matched anisotropic absorber for use as an absorbing boundary condition," *IEEE Transactions on Antennas and Propagation*, Vol. 43, 1460–1463, Dec. 1995.
35. Stupfel, B., "A study of the condition number of various finite element matrices involved in the numerical solution of Maxwell's equations," *IEEE Transactions on Antennas and Propagation*, Vol. 52, 3048–3059, Nov. 2004.
36. Michler, C., L. Demkowicz, J. Kurtz, and D. Pardo, "Improving the performance of perfectly matched layers by means of *hp*-adaptivity," *Numerical Methods for Partial Differential Equations*, Vol. 23, 832–858, Jul. 2007.
37. Pardo, D., L. Demkowicz, C. Torres-Verdin, and C. Michler, "PML enhanced with a self-adaptive goal-oriented *hp*-finite element method: Simulation of through-casing borehole resistivity measurements," *SIAM Journal of Scientific Computing*, Vol. 30, No. 6, 2948–2964, 2008.
38. García-Castillo, L. E., I. Gómez-Revuelto, F. Sáez de Adana, and M. Salazar-Palma, "A finite element method for the analysis of radiation and scattering of electromagnetic waves on complex environments," *Computer Methods in Applied Mechanics and*

Engineering, Vol. 194, Nos. 2–5, 637–655, Feb. 2005.

39. Chew, W. C., J. M. Jin, and E. Michielssen, "Complex coordinate stretching as a generalized absorbing boundary condition," *Microwave and Optical Technology Letters*, Vol. 15, 363–369, Sept. 1997.
40. Ubeda, E., J. M. Tamayo, and J. M. Rius, "Taylor-orthogonal basis functions for the discretization in method of moments of second kind integral equations in the scattering analysis of perfectly conducting or dielectric objects," *Progress In Electromagnetics Research*, Vol. 119, 85–105, 2011.
41. Bahadori, H., H. Alaeian, and R. Faraji-Dana, "Computation of periodic Green's functions in layered media using complex images technique," *Progress In Electromagnetics Research*, Vol. 112, 225–240, 2011.
42. Gómez-Revuelto, I., L. E. García-Castillo, and M. Salazar-Palma, "Goal-oriented self-adaptive *hp*-strategies for scattering and radiation problems," *Progress In Electromagnetics Research*, Vol. 125, 459–482, 2012.
43. Babuška, I. and B. Guo, "Approximation properties of the *hp*-version of the finite element method," *Computer Methods in Applied Mechanics and Engineering*, Vol. 133, 319–346, 1996.
44. Coifman, R., V. Rokhlin, and S. Wandzura, "The fast multipole method for the wave equation: A pedestrian prescription," *IEEE Antennas and Propagation Magazine*, Vol. 35, 7–12, Jun. 1993.
45. Eibert, T. F., Ismatullah, E. Kaliyaperumal, and C. H. Schmidt, "Inverse equivalent surface current method with hierarchical higher order basis functions, full probe correction and multi-level fast multipole acceleration," *Progress In Electromagnetics Research*, Vol. 106, 377–394, 2010.
46. Pan, X.-M., W.-C. Pi, and X.-Q. Sheng, "On OpenMP parallelization of the multilevel fast multipole algorithm," *Progress In Electromagnetics Research*, Vol. 112, 199–213, 2011.
47. Bebendorf, M., "Approximation of boundary element matrices," *Numerische Mathematik*, Vol. 86, No. 4, 565–589, 2000.